Molecular Doping and Band-Gap Opening of Bilayer Graphene

Alexander J. Samuels* **and J. David Carey**

Advanced Technology Institute, University of Surrey, Guildford, GU2 7XH, United Kingdom

ABSTRACT The ability to induce an energy band gap in bilayer graphene is an important development in graphene science and opens up potential applications in electronics and photonics. Here we report the emergence of permanent electronic and optical band gaps in bilayer graphene upon adsorption of π electron containing molecules. Adsorption of n- or p-type dopant molecules on one layer results in an asymmetric charge distribution between the top and bottom layers and in the formation of an energy gap. The resultant band gap scales linearly with induced carrier density though a slight asymmetry is found between n-type dopants, where the band gap varies as 47 meV/10^{13} cm^{-2}, and p-type dopants where it varies as 40 meV/10^{13} cm^{-2}. Decamethylcobaltocene (DMC, n-type) and 3,6-difluoro-2,5,7,7,8,8-hexacyanoquinodimethane (F2-HCNQ, p-type) are found to be the best molecules at inducing the largest electronic band gaps up to 0.15 eV. Optical adsorption transitions in the 2.8−4 μm region of the spectrum can result between states that are not Pauli blocked. Comparison is made between the band gaps calculated from adsorbate-induced electric fields and from average displacement fields found in dual gate bilayer graphene devices. A key advantage of using molecular adsorption with π electron containing molecules is that the high binding energy can induce a permanent band gap and open up possible uses of bilayer graphene in mid-infrared photonic or electronic device applications.

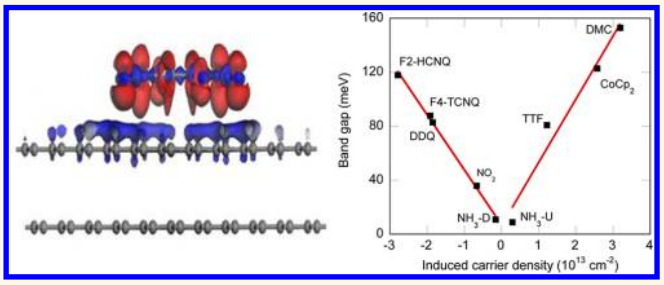

KEYWORDS: bilayer graphene · band-gap engineering · molecular doping · surface transfer doping · band structure · mid-infrared optical adsorption

Graphene and related materials have emerged as promising candidates for technological advances in a number of areas of electronics, photonics, and material science due to an impressive list of electronic,[1] transport[2], and optical[3] properties. The discovery of single layer graphene (SLG) has revealed a description of the carriers in terms of massless Dirac Fermions,[4] a new quantum Hall behavior,[5] and high carrier mobility.[1] Key to the successful application of a functional material in an electronic or photonic device is an ability to control the carrier concentration and for a number of electronic applications, especially digital switching applications, the zero band-gap nature of SLG remains problematic as it limits the on/off current ratio of graphene transistors. One dimensional graphene nanoribbons (GNRs) have been shown to possess a band gap inversely proportional to their width;[6] however, large scale production of high quality GNRs with the required precisely controlled edges[7] is yet to be realized. Devices fabricated using nanoperforated graphene sheets patterned by block copolymer lithography have been demonstrated[8] to achieve band gaps of 100 meV; however, these devices were found to have a relatively low carrier mobility of around 1 cm^2/(V s). Bernal (AB) stacked bilayer graphene (BLG) possesses a number of advantages over single layer graphene due to the ability to open an electronic band gap by breaking the inversion symmetry between the layers.[9] It is this fact that lies at the heart of much of bilayer graphene research for electronic and photonic applications.

The structure of bilayer graphene has been well documented and within a tight-binding description of AB stacking, electron hopping within the same layer between nearest neighbor atoms on different AB sublattices is characterized by the energy scale γ_0. In Bernal stacking the second layer is arranged such that A sublattice atoms in the upper layer (A2) are arranged above B sublattice atoms (B1) and characterized by hopping energy γ_1. Typical values of

* Address correspondence to A.Samuels@Surrey.ac.uk, David.Carey@surrey.ac.uk.

Received for review January 22, 2013 and accepted February 16, 2013.

Published online 10.1021/nn400340q

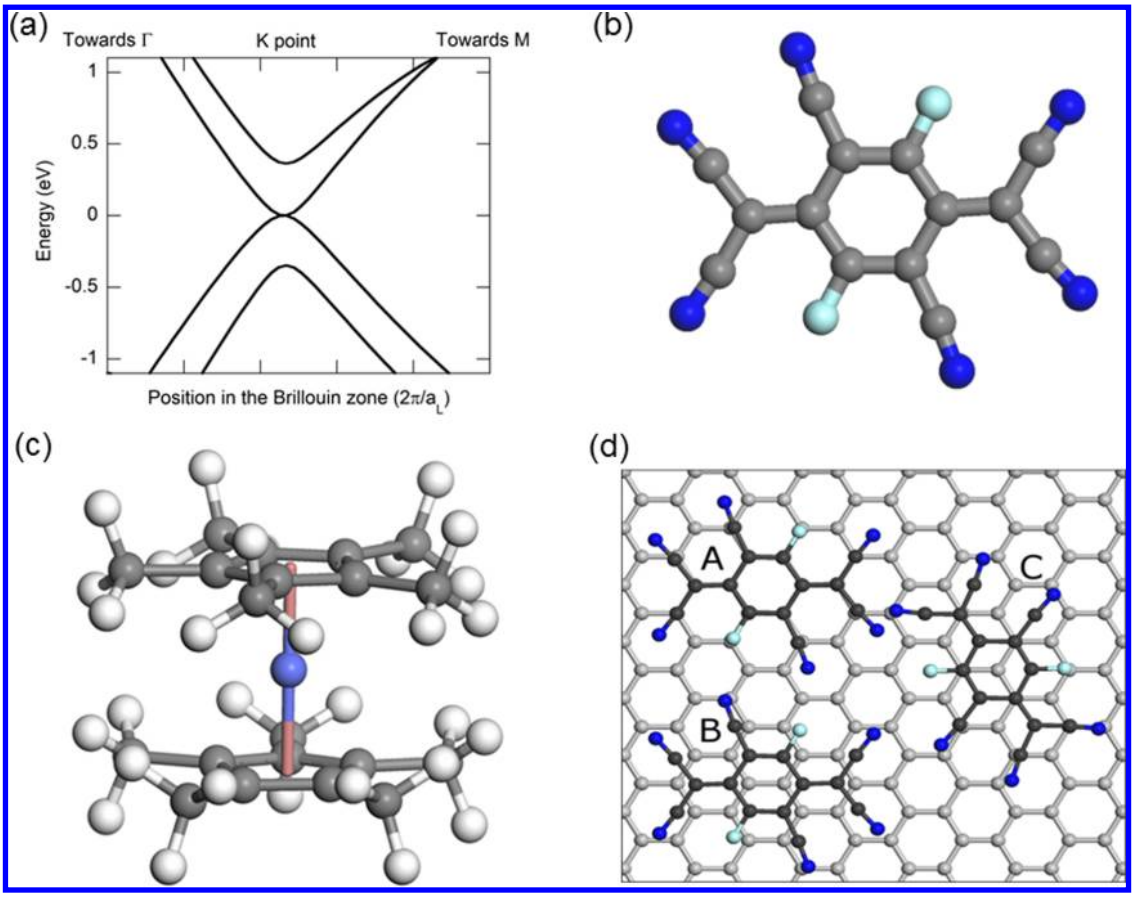

Figure 1. (a) Band structure of undoped bilayer graphene taken along the path from Γ to K to M points in the Brillouin zone using nonfolded notation. (b) Molecular structure of the F2-HCNQ molecule; carbon atoms (gray), nitrogen (dark blue), and fluorine (cyan). (c) Molecular structure of the DMC molecule; cobalt atom (light blue), carbon atoms (gray), and hydrogen atoms (white). (d) High symmetry adsorption geometries are characterized by the location of the central portion of the molecule over different arrangements of the carbon atoms in the top layer. Adsorption site A corresponds to adsorption over a hexagonal site, site B is adsorption over a carbon−carbon bond site and site C is adsorption over a carbon atom site. F2-HCNQ is shown as an example. Only one molecule per unit cell is performed per calculation.

γ_0 and γ_1 are about 3.4 eV and 0.35−0.4 eV, respectively.[10] Two other energy scales are of interest; γ_3 refers to hopping between A1−B2 sublattices and plays a role in trigonal warping of the Fermi surface contours; γ_4 refers to B1−B2 electron hopping and plays a role in electron−hole asymmetry and introduces an asymmetry in the shape of the bands and effective masses and it has been reported[10] to have a value of $(0.04-0.06)\gamma_0$. The band structure of undoped bilayer graphene consists of a pair of nested bands in each of the valence and conduction bands with the two lowest energy bands touching at the K points in the Brillouin zone (Figure 1a). The two higher bands are split off from each with a separation at K given by $2\gamma_1$. The point where the lowest energy bands touch is called the charge neutrality or Dirac point, analogous to that found in single layer graphene. The majority of previous efforts focused on opening an electronic band gap in bilayer graphene have used the application of displacement electric fields to induce an asymmetry in the on-site electron energies between the top and bottom layers.[11,12] This method, though limited by the SiO_2 gate dielectric breakdown field of 1 V/nm, has resulted in band gaps of up to 250 meV for charge neutral[12] BLG and up to 180 meV for doped BLG.[11]

An ability to control the carrier concentration is a key requirement for an electronic material. In the case of SLG this has been variously accomplished *via* decoration with metal adatoms,[13] substitutional doping with nitrogen or boron atoms,[14] edge modification using electrothermal reactions with ammonia,[15] decorating SLG with ultrathin layers of Si islands,[16] and surface transfer doping *via* the adsorption of large organic molecules,[17,18] with some of these methods resulting in the opening of a band gap in SLG. In the case of the latter study, ref 18, a 0.8 nm thick layer coating of tetrafluoro-tetracyanoquinodimethane (F4-TCNQ) was able to neutralize the substrate induced n-doping of epitaxial SLG grown on SiC and to shift the Fermi level by 0.42 eV. At intermediate and high surface coverage, the F4-TCNQ molecules were found to be oriented vertically on the layer. Only at low coverage was the plane of some of the molecules reported to be parallel to the graphene layer. Surface transfer doping, particularly with planar organic molecules, therefore offers

an attractive path to permanently modify the electronic properties in a controllable manner while introducing minimal structural deformations.

With the success of doping single layer graphene with π electron-containing molecules, we have extended this approach to bilayer graphene. We report charge transfer, changes to the carrier concentration, band structure, and density of states in Bernal stacked AB bilayer graphene using a range of molecules. We find that the high adsorption binding energies of π electron-containing molecules can permanently open both an electronic and optical band gap. The electrical band gaps are found to be comparable to those produced by dual date displacement fields and the optical gaps cover the important (atmospheric) $3-5\,\mu$m region and offer the opportunity of using BLG in photodetectors as a replacement of InSb, HgCdTe, and PbSe based devices. Indeed a dual gated BLG device has already been employed as a hot-electron bolometer for 10.6 μm detection with very low noise.[19] An added attraction of the use of molecular dopants in the vicinity of the graphene layers is that adsorption does not introduce significant phonon scattering often found with high atomic mass oxides used as substrates. Our goal in this study is to explore what factors control the magnitude of the band gap in doped bilayer graphene and unlike previous studies, which have employed a single type of molecule, for example in the use of benzyl viologen,[20] we employ a range of p- and n-type dopant molecules, quantify the degree of charge transfer and carrier density and relate to both optical and electrical band gaps. We also compare the size of the band gap found from the adsorbate induced internal electric field between the layers with those induced by average displacement fields in dual gate devices.

We have selected technologically important molecules, previously successfully used in organic electronics. For example, 3,6-difluoro-2,5,7,7,8,8-hexacyanoquinodimethane (F2-HCNQ, Figure 1b) has been shown to exhibit superior p-type doping characteristics of organic thin films and improved thermal stability[21] when compared to the commonly used F4-TCNQ. Molecules possessing π electrons, such as F2-HCNQ, will be important in controlling the adsorption energies due to effective $\pi-\pi$ stacking interactions[22] and the charge transfer. For example, each CN group of F2-HCNQ contributes 4 π electrons to a total of 32 π electrons per molecule where the high number of electronegative cyano CN functional groups result in the strong electron withdrawing character. Another important molecule is decamethylcobaltocene (Figure 1c) which consists of a cobalt atom sandwiched between two methyl-substituted cyclopentadienyl groups and has previously been demonstrated as an efficient n-type dopant in organic electronic materials and devices, due to its extremely low solid-state ionization energy of 3.3 eV.[23] Like its unsubstituted parent compound cobaltocene ($CoCp_2$), DMC is a spin-polarized molecule with 19 valence electrons. While we will concentrate on the effects of the adsorption of F2-HCNQ and DMC, we have also examined the effects of other molecules such as $CoCp_2$, TTF (tetrathiafulvalene), NH_3, F4-TCNQ, DDQ (2,3-dichloro-5,6-dicyano-1,4-benzoquinone), and NO_2 and report the effects of the adsorption of each of the molecules.

TABLE 1. Optimum Intermolecular Separation (d), Binding Energy (E_b), and Electron Charge Transfer (Q) for F2-HCNQ Adsorbed on AB Stacked Bilayer Graphene[a]

adsorption site	d (Å)	E_b (eV)	Q (e)
A	3.24	1.72	0.53
B	3.14	1.82	0.51
C	3.14	1.90	0.51

[a] The electron charge transfer is calculated from the Hirshfeld charge partitioning and positive values for Q indicate p-type doping. The intermolecular separation is measured from the centre-of-mass of the molecule to the top layer of the bilayer graphene.

RESULTS AND DISCUSSION

Our density functional theory (DFT) calculations of the undoped band structure of BLG (Figure 1a) reveal a value of γ_1 of 0.36 eV. From the low energy dispersion we also find that the electron and hole effective masses to be $0.046m_0$ and $0.053m_0$, respectively.

F2-HCNQ Adsorption on Bilayer Graphene. From Table 1, it is evident that the optimum intermolecular separation, binding energy, and electron charge transfer are similar for the different adsorption sites of F2-HCNQ adsorbed on one surface of bilayer graphene. With the center hexagon of the F2-HCNQ molecule above the hexagonal site (site A) of the top graphene layer the optimum intermolecular separation is 0.10 Å further away than in the preferred highest binding energy bond site position (site B) and the binding energy is reduced from 1.82 to 1.72 eV. During geometry optimization with the F2-HCNQ molecule above the carbon atom site (site C), the molecule was found to migrate toward site B, suggesting a strong preference for the bond site. The calculated high binding energies for F2-HCNQ on bilayer graphene are associated with a strong $\pi-\pi$ stacking interaction.

We believe that the binding energy depends on the relative arrangement of the atoms in the molecule to the atoms in the BLG. For example site C, in Figure 1d, where the central molecule hexagon is over an atom is reminiscent of Bernal AB stacking (hence high binding energy). In site A, the arrangement of the atoms in the molecule top layer is similar to the less favored AA stacking. This arrangement is energetically unfavorable and would raise the total energy of the system and result in a lower binding energy. However much of the charge transfer is associated with the cyano groups, which are not over particular carbon sites; hence, the

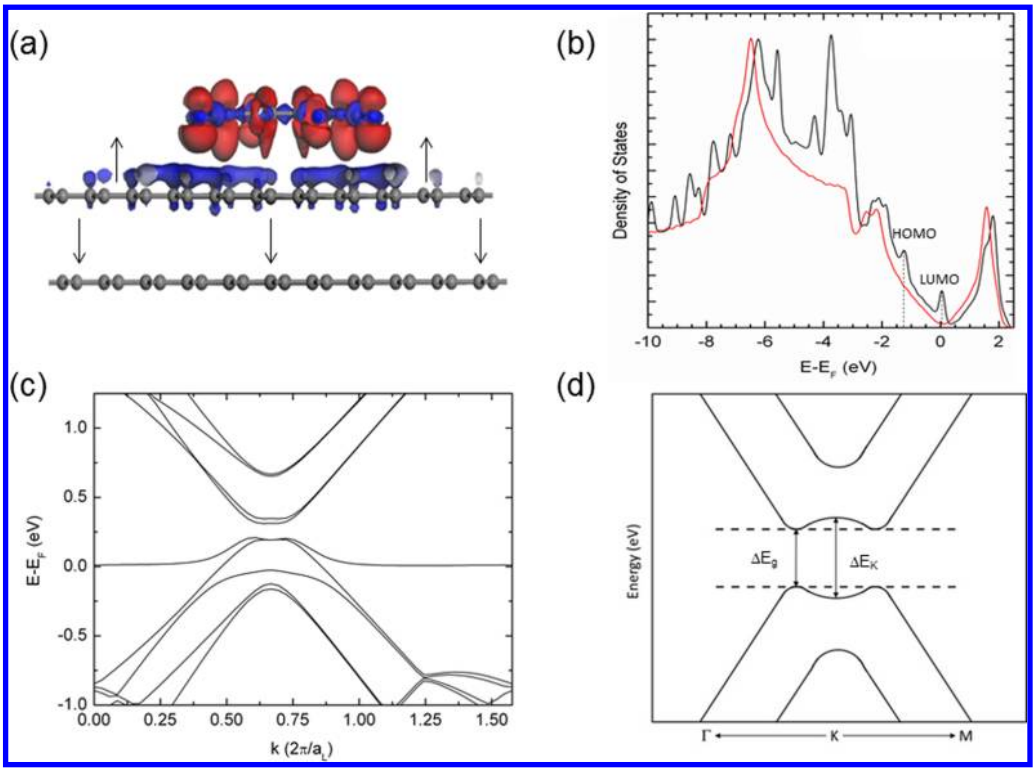

Figure 2. (a) Isosurface of the change in electron density surrounding bilayer graphene with an absorbed F2-HCNQ molecule (isovalue $\pm 5 \times 10^{-3}$ e/Å^3). Red and blue regions show areas of increasing and decreasing electron density, respectively. The arrows show the direction of the electric field internal to the bilayer layer and also from the top layer to the molecule due presence of positively charged holes on the top surface. (b) Density of states of undoped bilayer graphene (red line) and bilayer graphene doped with an F2-HCNQ molecule (black line). The LUMO level of F2-HCNQ lies 0.21 eV below E_D facilitating electron charge transfer from the BLG to the F2-HCNQ molecule. (c) Band structure of a 6 × 6 bilayer graphene supercell with an adsorbed F2-HCNQ molecule. (d) Schematic band structure model of doped BLG close to the K point showing the "Mexican hat" dispersion.

similarity of the charge transfers. Tian, Xu, and Wang[24] observed that with F4-TCNQ at low coverage the binding energy ranges from 1.8 to 1.95 eV depending on relative changes of position, so the variation quoted in Table 1 is of a similar amount. Upon adsorption the bond lengths of the C−N triple bonds in the four outer cyano groups are found to increase from 1.166 to 1.168 Å, the inner cyano groups also increase their bond lengths from 1.163 to 1.165 Å and the C−F bonds increase from 1.318 to 1.326 Å, confirming electron withdrawal from BLG. The values of the charge transfer between the different adsorption site are similar with only 0.02 electrons/molecule difference between sites A, B, and C. The electron charge transfer of 0.51 electrons/molecule from the bilayer graphene to the F2-HCNQ molecule corresponds to a significant increase in hole carrier concentration of 2.7×10^{13} cm^{-2}. Using a dispersion corrected GGA functional (GGA-TS) (details in the method section) we have calculated a doping efficiency of 0.53 electrons/molecule. These results are in good agreement with those calculated using the LDA functional. We have also tested the commonly used molecule F4-TCNQ adsorbed on BLG and found that by using the same concentration of dopant molecules the charge transfer to the F4-TCNQ molecule was 0.36 electrons/molecule with a binding energy of 1.55 eV. Sun *et al.* reported[25] the adsorption of F4-TCNQ on SLG to be 0.4e per molecule with a binding energy of 1.28 eV, whereas for the case of adsorption on BLG, Tian *et al.* reported[24] a charge transfer of 0.45e per molecule with a binding energy of 1.39 eV. Our results confirm the superiority of F2-HCNQ, in terms of binding energy (1.90 eV) and charge transfer (0.5e), as a permanent p-type dopant for bilayer graphene. We believe that the enhanced p-type doping found with F2-HCNQ is due to the higher number of cyano groups of the former.

From Figure 2a it can be seen that the majority of this transferred charge to the F2-HCNQ molecule is from the top BLG layer as well as some charge redistribution surrounding the molecule (red and blue areas). From the density of states (Figure 2b) it can be seen that the lowest unoccupied molecular orbital (LUMO) level of F2-HCNQ lies 0.21 eV below the charge neutrality Dirac point, thus enabling direct electron transfer from the states close to E_D to the LUMO of F2-HCNQ. The resulting charge difference between the top and bottom layers results in a net in-built electric field. The band structure of graphene with adsorbed F2-HCNQ is shown in Figure 2c where the Fermi level (E_F)

TABLE 2. Optimum Intermolecular Separation (d), Binding Energy (E_b), and Electron Charge Transfer (Q) Data for DMC Adsorbed on AB Stacked Bilayer Graphene[a]

adsorption site	d (Å)	E_b (eV)	Q (e)
A	5.04	2.02	−0.60
B	5.05	1.85	−0.60
C	5.05	1.97	−0.53

[a] Electron charge transfer calculated from the Hirshfeld charge partitioning, negative values for Q indicate n-type doping.

is shifted downward into the valence band by approximately 0.25 eV consistent with the p-type doping calculated earlier and the emergence of a band gap close to the neutrality point. The horizontal line in Figure 2c is the molecular impurity level associated with the adsorption of the molecule. In this case the impurity level crosses with the graphene band, and this level should be considered to be in the bilayer graphene valence band. Because of the "Mexican hat" dispersion,[9] it is necessary to carefully define the band gap with Figure 2d showing how the separation between the conduction and valence bands is slightly wider at the K point. Upon adsorption of F2-HCNQ the calculated band gap (ΔE_g) is 118 meV and the band separation at the K point (ΔE_K) is 121 meV. We find that the values of ΔE_g and ΔE_K agree within a tight-binding description,[26] taking γ_1 to be the previously calculated value in undoped BLG of 0.36 eV,

$$\Delta E_g = \frac{\Delta E_K \gamma_1}{(\Delta E_K{}^2 + \gamma_1{}^2)^{1/2}} \quad (1)$$

Given the size of the band gap it is possible to estimate the strength of the resultant in-built electric field, E_i, arising from the adsorbate induced asymmetric charge distributions. Within a tight-binding description a (screened) in-built field can be approximated as

$$E_i \approx \frac{\Delta E_K}{d} \quad (2)$$

where d is the separation between the top and bottom layers of the bilayer graphene.[26] In the case of a 6 × 6 supercell of bilayer graphene with a single adsorbed F2-HCNQ molecule the in-built electric field is calculated to be 0.36 V/nm, assuming a 3.35 Å separation between the layers.

Decamethylcobaltocene on Bilayer Graphene. The adsorption of DMC onto one surface of BLG occurs with a high binding energy, Table 2, of 1.85−2.02 eV, with a 0.17 eV difference in binding energy between the most stable site (site A) and the least stable site (site B). The high binding energy of the DMC molecule to bilayer graphene can also be attributed to a strong $\pi-\pi$ interaction as DMC has 12 π electrons (6 from each substituted cyclopentadienyl ring). The optimum intermolecular separation (measured from the center of the molecule at the cobalt atom to the top layer of the bilayer graphene) is almost identical for the different adsorption sites at 5.04−5.05 Å. After adsorption the structure of the DMC molecule is found to change slightly with the Co−Cp bond (cobalt atom to the center of the substituted ring) shortening from 1.678 to 1.627 Å, consistent with electron donation. Indeed a high electron charge transfer of 0.60 electrons/molecule transferred to the BLG is calculated when the molecule is adsorbed in the most stable adsorption site (A), resulting in a carrier concentration of 3.2 × 10^{13} cm^{-2}. To induce the same carrier concentration using a standard gated device configuration on a 300 nm SiO_2 substrate would require a gate voltage in excess of 440 V (assuming a gate efficiency of 7.2 × 10^{10} cm^{-2}/V), which would exceed the breakdown field for SiO_2 of 1 V/nm.

From Figure 3a it can be seen that the spin-polarized highest occupied molecular orbital (HOMO) and LUMO levels of DMC are closely spaced separated by only 78 meV. The small energy separation between the HOMO and LUMO in DMC is characteristic of open-shell molecules with an odd number of electrons where the energy levels are exchange split. The HOMO level lies 0.75 eV above E_D of bilayer graphene, and this enables efficient direct transfer of electrons to the unoccupied π^* states. For comparison the adsorption of unsubstituted cobaltocene, which is also considered to be an effective n-type dopant, was calculated to have a doping efficiency of 0.49 electrons/molecule showing the increased effectiveness of the methyl-substituted DMC as an n-type dopant for BLG. From the isosurface of the change in electron density (Figure 3b) it is clear that the transferred electron charge is more tightly localized below the DMC molecule than in the case of the holes induced by adsorption of F2-HCNQ. There is noticeable charge redistribution within the DMC molecule as the spin-polarized HOMO of DMC changes from being fully occupied to partially occupied. Once again the majority of the induced charge carriers remain on the top bilayer, resulting in a charge difference between the top and bottom layers and therefore an in-built electric field. The band structure of DMC doped BLG, which can be seen in Figure 3c, shows an upward Fermi level shift of approximately 0.3 eV, consistent with strong n-type doping and the emergence of a 153 meV band gap. The energy gap at the K point is found to be 181 meV and from eq 2 we find an in-built electric field of 0.54 V/nm.

The horizontal line spanning the band structure in Figure 3c is the impurity level associated with the adsorption of the DMC molecule. Note the slight splitting of where this line and bands cross is associated with the spin-polarized nature of the molecule. Unlike that seen in Figure 2c, the impurity level is in the conduction band of BLG making this a n-type BLG layer which has implications for the allowed optical transitions. Optical adsorption transitions are possible in

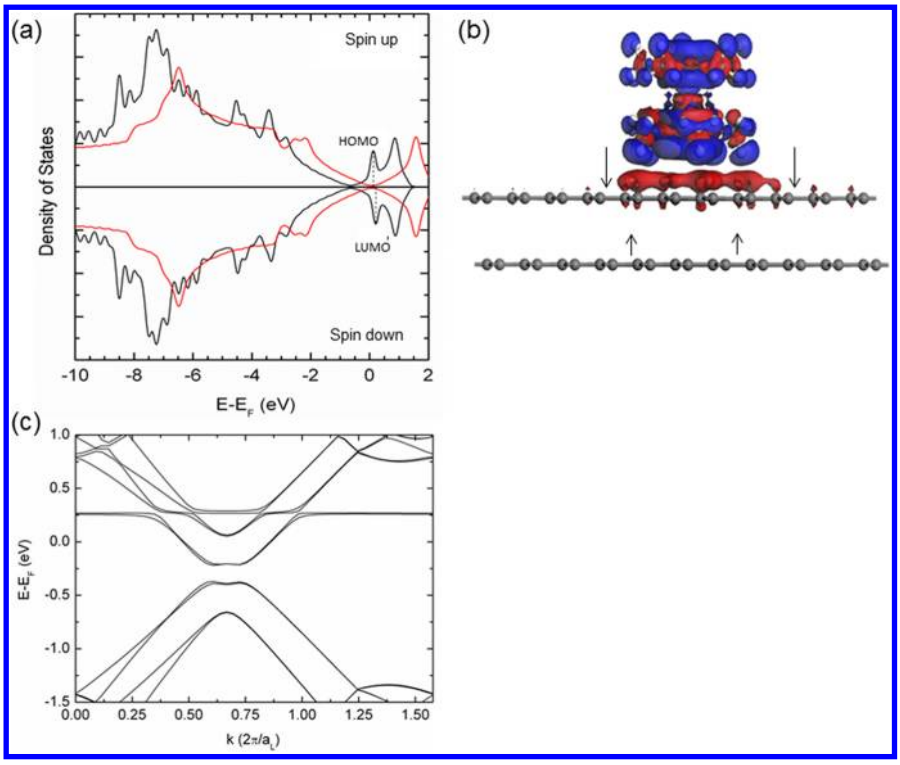

Figure 3. (a) Spin-polarized density of states of undoped bilayer graphene (red lines) and bilayer graphene with an adsorbed DMC molecule (black lines). (b) Isosurface of the change in electron density with an adsorbed DMC molecule (isovalue $\pm 4 \times 10^{-3}$ e/Å^3). Red areas show increased electron density and blue shows areas of electron depletion, respectively. The arrows show the direction of the electric field internal to the bilayer layer and also from the top layer to the molecule due to the presence of negatively charged electrons on the top surface. (c) Band structure of a 6 × 6 AB stacked bilayer graphene supercell with an absorbed DMC molecule. A band gap of 153 meV can be observed (181 meV at the neutrality point) and E_F is shifted upward by 0.30 eV with respect to undoped bilayer graphene.

DMC-doped BLG with transitions from the filled to unfilled states and the location of the Fermi level relative to each band will determine if the transition will occur or is Pauli blocked and at what energy. In the case of adsorption of DMC, the band structure of Figure 3c shows that adsorption transitions in the 259−307 meV and 442−466 meV range are possible as the Fermi level is above the first conduction band but below the second conduction band. Similarly in the case of F2-HCNQ the transitions (Figure 2c) from 315 to 335 meV and around 436 meV are possible. These transitions cover the 2.8−4 μm region and show that the doped BLG could be selectively used in mid-infrared photonics.

Finally, in Figure 4a we report the variation of the electronic band gap with induced carrier concentration for all the molecules investigated using the same concentration of one molecule per bilayer graphene supercell. Similar to the case of doping single layer graphene, the p-type dopants F4-TCNQ and DDQ are seen to have very similar doping efficiencies of 0.36 and 0.35 electrons/molecule transferred, respectively, with resultant band gaps of 88 and 83 meV. It can also be seen that the larger organic and organometallic molecules act as far more efficient dopants than the smaller molecules, such as NO_2 and ammonia. The binding energy of the organic and organometallic molecules is also an order of magnitude greater than that of the smaller molecules; we calculate, for example, a binding energy of 0.24 eV for ammonia, therefore showing organic and organometallic molecules to be superior for the stable doping and the opening of a permanent band gap in BLG. Ammonia adsorption on bilayer graphene is found to exhibit amphoteric behavior with n-type doping found with the N atom pointing to the bilayer and p-type doping with the H atoms closer to the bilayer.

For both p-type and n-type dopants, there are good linear fits of increasing band gap with carrier concentration with a slight asymmetry between n-type and p-type carriers. The slope with p-type dopants is found to be 40 meV/10^{13} cm^{-2} carriers while the slope for n-type bilayer graphene is 47 meV/10^{13} cm^{-2}. Zhang *et al.* measured a variation of 70 meV/10^{13} cm^{-2} using different concentrations of oxygen/moisture and a protective layer of triazine.[27] We believe that the asymmetric behavior of the band gap with carrier concentration is due to the asymmetric shape of the conduction and valence bands due to nonzero γ_4 hopping. It is interesting to note that we find the ratio of hole to electron effective masses found in undoped BLG to be 1.15, which is similar to the inverse of the

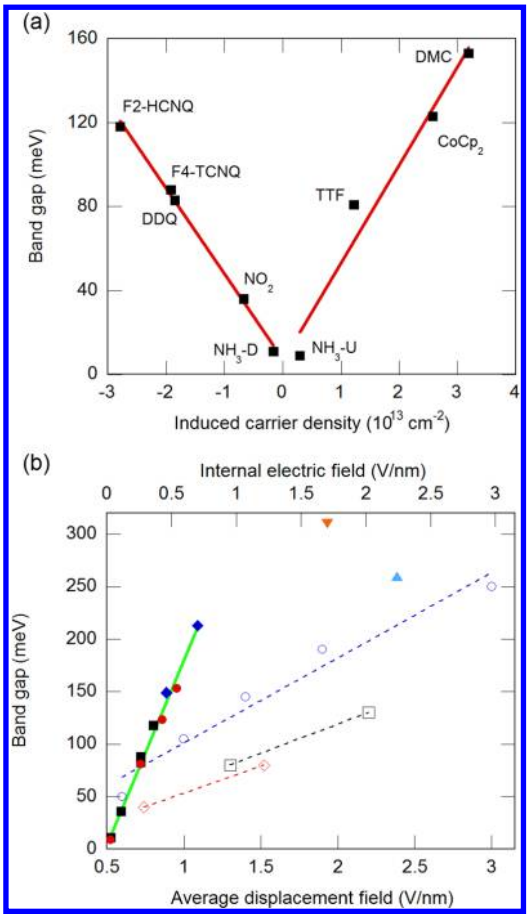

Figure 4. (a) Electronic band gap as a function of carrier concentration induced by a number of different molecules indicated; NH_3-D (-U) corresponds to an ammonia molecule adsorbed with the hydrogen atoms closer to (further from) the top layer. (b) Variation of electrical band gap with adsorbate-induced internal electric field with n-type (red ●) and p-type (black ■) dopants from this study and from Tian *et al.* (blue ♦) (ref 24). The solid green line is a linear fit to the data through the three sets of data. Values of band gap from dual molecular adsorption from Duong *et al.* (orange ▼) ref 30 and Cuong *et al.* (blue ▲) ref 31. Variation with band gap with average displacement fields from Zhang *et al.* (blue ○) ref 12, from Szafranek *et al.* (black □) ref 28 and from Xia *et al.* (red ◊) ref 29. The dashed lines are linear guides to the eye.

ratio of the variation of band gap with carrier concentration for p-type and n-type dopants (1.18).

The band gaps calculated here can be compared with those reported from studies of dual gate devices. Electrical band gaps can be induced in BLG using displacement fields associated with the top and bottom electrodes on the top and bottom layers, D_t and D_b, respectively, with

$$D_t = \frac{\varepsilon_t(V_t - V_t^0)}{d_t} \quad \text{and} \quad D_b = \frac{\varepsilon_b(V_b - V_b^0)}{d_b} \qquad (3)$$

where $\varepsilon_{t(b)}$ is the dielectric constant of the insulator separating the top (bottom) electrode from the BLG layer, $V_{t(b)}$ is the voltage applied to the top (bottom) electrode in the presence of any offset voltages, $V^0_{t(b)}$, due to residual atmospheric or processing doping. The average displacement field, $D_{ave} = {}^1/_2(D_t + D_b)$, is responsible for breaking inversion symmetry of the electron on-site energies and the appearance of a band gap. A nonzero difference in fields ($D_t - D_b$) results in a shift of the Fermi level and intentional doping. Figure 4b shows the electronic band gap as a function of average displacement fields from a number of experimental studies using dual gate electrode geometries[14,28,29] and internal electric fields determined from this study and some reported in the literature using dual molecule doping.[30,31] The difference between the values of the fields required is a reflection of the screened nature of adsorbate induced electric fields and the displacement fields. This is seen in the variation of the band gap with an average displacement field which scales as 51−81 meV/V/nm, whereas it scales as 296 meV/V/nm with internal electric field. The topic of screening in bilayer layers has been the subject of considerable discussion in the literature.[9,32] For example, Gava *et al.*[32] calculated that in the absence of electronic screening the band gap (meV) scales as $30 \times 10^{-12} \times$ (net carrier density) per unit area (cm^{-2}). When the effects of screening are included, this reduces by a factor of 4−4.3 for carrier densities of $(1-2) \times 10^{13}$ cm^{-2}, similar to those found here.

From Figure 4b it is apparent that the use of dopant molecules is able to produce an electronic gap comparable to those produced using a dual gate geometry, which in turn should affect the transistor device characteristics. For example, in the study by Szafranek *et al.*,[28] with a D_{ave} of 1.7 V/nm using Al as a dopant, transistor on/off ratios of between 30 and 40 were measured. Lower on/off ratios (5−20) were found with devices exposed to atmospheric dopants with back gate displacement fields of 0.8 V/nm. Using molecular dopants, where the surface covering can be more accurately controlled, should lead to higher on/off ratios accompanied by a lower spread in device performance. Xia *et al.* reported[29] a room temperature on/off ratio of 100 with an electrical band gap of over 130 and 80 meV at average displacement fields of 2.3 and 1.3 V/nm, respectively. Their BLG devices employed the deposition of 9 nm polymeric layer before HfO_2 was deposited by atomic layer deposition. Such a polymeric layer decouples the graphene layer from the presence of remote interface polar phonons from the oxide substrate which can act as strong scattering centers. The use of organic molecules, which can be put down by solution processing, wet chemistry methods along with polymeric insulating layers should also have the same advantageous behavior.

It is also possible to combine both molecular doping and the application of an electric field to increase the band gap still further. In the study by Tian *et al.*,[24] a value of ΔE_G of 213 meV increased to 253 meV in an external field of 0.77 V/nm. The corresponding value of ΔE_K and built-in field were 236 meV and 0.7 V/nm

under zero bias and 306 meV and 0.95 V/nm under external field, respectively. From Figure 4b the variation of band gap for the n- and p-type dopants in this study and the F4-TCNQ at high and low coverage appear to follow the same trend (solid green line) with internal electric field with a slope of about 296 meV/V/nm. Increasing the band gap even further is possible by using two different molecules in which one molecule is used to dope one side of a BLG layer n-type and another molecule is able to dope the other side p-type and can increase the size of the band gap—so-called dual molecule doping. For example, Duong *et al.*[30] used a benzyl viologen (BV, n-type)−bis(trifluoromethylsulfonyl)imide (TFSI, p-type) pair to induce a reported band gap of 0.31 eV at an internal field of 1.7 V/nm. Cuong *et al.*[31] recently used three types of cation−anion pair and calculated a band gap of between 0.26 and 0.32 eV. For the case of a tetrafluoroborate (BF_4^-) anion/1-ethyl-1-methyl pyrrolidinum cation pair the band gap of 0.26 eV was found at an internal field of 2.2 V/nm. These data are also reported in Figure 4b; however, the presence of ionic molecules may affect the electrical conductivity of the BLG layer as they may increase charged impurity and resonant scattering. In both of the latter two studies it was noted that the Fermi level could be shifted in to the band gap thereby producing an intrinsic semiconductor. Single molecule doping, as in this study, although easier to implement tends to result in the impurity bands being located in either the valence or conduction band, as in Figures 2c and 3c. Dual molecule doping with a Fermi level in the middle of the bands results in a net lower carrier concentration. It would allow more optical transitions to occur where there is less Pauli blocking of states.

Molecular doping, using either single or dual species, has the added advantage of not inducing structural defects into the carbon lattice. Zhao and Xue[33] recently employed B or N ion implantation into BLG and reported a band gap of 392 meV. However the substituted B or N ion in the top BLG layer was accompanied by knock on of a C atom to form a carbon−carbon dumbbell defect on the lower layer. The formation energy of the B (N)−dumbell defect complex was calculated, *via* DFT, to be 11 eV (7.1 eV) which would require a nonequilibrium technique, such as ion implantation to implement. These authors highlighted that ion implantation as a technique could also result in the creation of sp^3 defects which could aid in cross-linking of the graphene layers; however from a transport perspective it may reduce mobility and introduce resonant scattering centers. As such despite the attractiveness of ion implantation as a mature technique to modify the properties of the layers, it may introduce significant detrimental effects in terms of electrical behavior. Solution deposition of organic molecules may therefore have a significant advantage for large area bilayer graphene science and technology to improve electrical conduction and allow the use of BLG as conductive electrode materials as well as open an energy gap for transistor and mid-infrared photonic applications.

SUMMARY AND CONCLUSIONS

Using *ab initio* DFT calculations we have shown that a number of organic and organometallic molecules can be utilized in order to dope bilayer graphene and open an energy gap. We have also demonstrated the superiority of F2-HCNQ and DMC over the commonly used F4-TCNQ and cobaltocene molecules. These molecules are found to adsorb with high binding energies enabling a stable doping method for bilayer graphene-based devices. By decorating one side of bilayer graphene it is possible to induce a permanent electronic band gap of up to 150 meV. The electronic band gap is found to vary as 40 meV/10^{13} cm^{-2} for p-type doping and 47 meV/10^{13} cm^{-2} for n-type doping. The opening of a permanent band gap in BLG will help to improve the on/off current ratio of graphene-based transistors and a tunable band gap in the mid-infrared region enables the development of graphene-based photonic detectors.

METHODS: COMPUTATIONAL DETAILS

The *ab initio* calculations are performed within the DMol[3] code based on density functional theory. The bilayer graphene supercell is modeled using a 6 × 6 unit cell, lattice constant $a_L = 6a_0$ (where a_0 is the graphene unit cell lattice constant 2.461 Å) with 144 carbon atoms (72 C atoms per layer, area per layer of 188.82 $Å^2$) and 3.35 Å interlayer separation. A vertical spacing of 20 Å between pairs of graphene bilayers has been used in order to avoid self-interaction. The Brillouin zone has been integrated using a 5 × 5 × 1 Monkhorst-Pack[34] grid for geometry optimization, binding energy, and charge transfer calculations and a finer 10 × 10 × 1 grid has been employed for the calculation of the density of states and band structure. The high symmetry points in the band structure are labeled in nonreduced notation. The local density approximation (LDA) functional of Vosko, Wilk, and Nusair[35] has been utilized for the majority of the results presented here. Although neither the LDA, nor the generalized gradient approximation (GGA), functional fully account for van der Waals (vdW) interactions, the LDA functional has been shown to perform well for adsorption on graphene and weakly bound systems,[36,37] such as those under consideration here. For the sake of comparison we have also performed benchmark calculations using a vdW-corrected GGA functional of Perdew, Burke, and Ernzerhof[38] with a dispersion correction devised by Tkatchenko and Scheffler.[39] Only a limited number of dispersion-corrected DFT calculations have been completed due to the computational cost of these calculations.

All calculations of electron charge transfer were performed using the Hirshfeld charge partitioning method.[40] A double numerical plus polarization (DNP) basis set has been employed to describe the molecular orbitals with an all-electron core treatment. An orbital cutoff has been applied to give atomic energies that are within 0.1 eV/atom of their reference values. All geometry optimizations were converged such that the maximum force on any atom in the system was less than

0.04 eV/Å. Three different adsorption high symmetry sites above the top graphene layer have been investigated with the center of the molecule above a hexagonal site of the top layer (site A), above a carbon−carbon bond site (site B), and above a carbon atom in the top layer of the BLG (site C), as shown in Figure 1d. The potential energy is the difference between the energy of the combined BLG−molecule system at the optimum intermolecular separation and the total energy of the BLG and molecule on its own.

$$E_{\text{potential}} = E_{\text{total}} - E_{\text{graphene}} - E_{\text{molecule}} \quad (4)$$

The binding energy is defined as the magnitude of the minimum potential energy at the optimum intermolecular separation where the intermolecular separation is taken from the center-of-mass of the molecule to the graphene layer. The electron density difference is the difference between the electron density surrounding the BLG in the presence and absence of the molecule.

Conflict of Interest: The authors declare no competing financial interest.

Acknowledgment. A.J.S. would like to acknowledge EPSRC Postgraduate Studentship support. J.D.C. acknowledges previous support from EPSRC.

REFERENCES AND NOTES

1. Novoselov, K. S.; Geim, A. K.; Morozov, S. V; Jiang, D.; Zhang, Y.; Dubonos, S. V.; Grigorieva, I. V.; Firsov, A. A. Electric Field Effect in Atomically Thin Carbon Films. *Science* **2004**, *306*, 666–669.
2. Mayorov, A. S.; Gorbachev, R. V.; Morozov, S. V.; Britnell, L.; Jalil, R.; Ponomarenko, L. A.; Blake, P.; Novoselov, K. S.; Watanabe, K.; Taniguchi, T.; *et al*. Micrometer-Scale Ballistic Transport in Encapsulated Graphene at Room Temperature. *Nano Lett.* **2011**, *11*, 2396–2399.
3. Wang, F.; Zhang, Y.; Tian, C.; Girit, C.; Zettl, A.; Crommie, M.; Shen, Y. R. Gate-Variable Optical Transitions in Graphene. *Science* **2008**, *320*, 206–209.
4. Novoselov, K. S.; Geim, A. K.; Morozov, S. V.; Jiang, D.; Katsnelson, M. I.; Grigorieva, I. V.; Dubonos, S. V.; Firsov, A. A. Two-Dimensional Gas of Massless Dirac Fermions in Graphene. *Nature* **2005**, *438*, 197–200.
5. Zhang, Y.; Tan, Y.-W.; Stormer, H. L.; Kim, P. Experimental Observation of the Quantum Hall Effect and Berry's Phase in Graphene. *Nature* **2005**, *438*, 201–204.
6. Han, M.; Özyilmaz, B.; Zhang, Y.; Kim, P. Energy Band-Gap Engineering of Graphene Nanoribbons. *Phys. Rev. Lett.* **2007**, *98*, 206805.
7. Wang, X.; Ouyang, Y.; Li, X.; Wang, H.; Guo, J.; Dai, H. Room-Temperature All-Semiconducting sub-10 nm Graphene Nanoribbon Field-Effect Transistors. *Phys. Rev. Lett.* **2008**, *100*, 100–103.
8. Kim, M.; Safron, N. S.; Han, E.; Arnold, M. S.; Gopalan, P. Fabrication and Characterization of Large-Area, Semiconducting Nanoperforated Graphene Materials. *Nano Lett.* **2010**, *10*, 1125–1131.
9. McCann, E. Asymmetry Gap in the Electronic Band Structure of Bilayer Graphene. *Phys. Rev. B* **2006**, *74*, 161403.
10. Zou, K.; Hong, X.; Zhu, J. Effective Mass of Electrons and Holes in Bilayer Graphene: Electron−Hole Asymmetry and Electron−Electron Interaction. *Phys. Rev. B* **2011**, *84*, 085408.
11. Mak, K.; Lui, C.; Shan, J.; Heinz, T. Observation of an Electric Field Induced Band Gap in Bilayer Graphene by Infrared Spectroscopy. *Phys. Rev. Lett.* **2009**, *102*, 100–103.
12. Zhang, Y.; Tang, T.-T.; Girit, C.; Hao, Z.; Martin, M. C.; Zettl, A.; Crommie, M. F.; Shen, Y. R.; Wang, F. Direct Observation of a Widely Tunable Band gap in Bilayer Graphene. *Nature* **2009**, *459*, 820–823.
13. Chen, J.-H.; Jang, C.; Adam, S.; Fuhrer, M. S.; Williams, E. D.; Ishigami, M. Charged-Impurity Scattering in Graphene. *Nat. Phys.* **2008**, *4*, 377–381.
14. Panchakarla, L. S.; Subrahmanyam, K. S.; Saha, S. K.; Govindaraj, A.; Krishnamurthy, H. R.; Waghmare, U. V.; Rao, C. N. R. Synthesis, Structure, and Properties of Boron- and Nitrogen-Doped Graphene. *Adv. Mater.* **2009**, *21*, 4726–4730.
15. Wang, X.; Li, X.; Zhang, L.; Yoon, Y.; Weber, P. K.; Wang, H.; Guo, J.; Dai, H. N-Doping of Graphene through Electrothermal Reactions with Ammonia. *Science* **2009**, *324*, 768–771.
16. Lee, D. H.; Yi, J.; Lee, J. M.; Lee, S. J.; Doh, Y.-J.; Jeong, H. Y.; Lee, Z.; Paik, U.; Rogers, J. A.; Park, W. I. Engineering Electronic Properties of Graphene by Coupling with Si-Rich, Two-Dimensional Islands. *ACS Nano* **2013**, *7*, 301–307.
17. Wang, X.; Xu, J.-B.; Xie, W.; Du, J. Quantitative Analysis of Graphene Doping by Organic Molecular Charge Transfer. *J. Phys. Chem. C* **2011**, *115*, 7596–7602.
18. Coletti, C.; Riedl, C.; Lee, D. S.; Krauss, B.; Patthey, L.; von Klitzing, K.; Smet, J. H.; Starke, U. Charge Neutrality and Band-Gap Tuning of Epitaxial Graphene on SiC by Molecular Doping. *Phys. Rev. B* **2010**, *81*, 235401.
19. Yan, Y.; M.-H. Kim, M.-H.; Elle, J. A.; Sushkov, A. B.; Jenkins, G. S.; Milchberg, H. M.; Fuhrer, M. S.; Drew, H. D. Dual-Gated Bilayer Graphene Hot Electron Bolometer. *Nat. Nanotechnol.* **2012**, *7*, 472–478.
20. S Yu, W. J.; Liao, L.; Chae, S. H.; Lee, Y. H.; Duan, X. Toward Tunable Band Gap and Tunable Dirac Point in Bilayer Graphene with Molecular Doping. *Nano Lett.* **2011**, *11*, 4759–4763.
21. Gao, Z. Q.; Mi, B. X.; Xu, G. Z.; Wan, Y. Q.; Gong, M. L.; Cheah, K. W.; Chen, C. H. An Organic p-Type Dopant with High Thermal Stability for an Organic Semiconductor. *Chem. Commun.* **2008**, 117–119.
22. Bjork, J.; Hanke, F.; Palma, C.-A.; Samori, P.; Cecchini, M.; Persson, M. Adsorption of Aromatic and Anti-aromatic Systems on Graphene through $\pi-\pi$ Stacking. *J. Phys. Chem. Lett.* **2010**, *1*, 3407–3412.
23. Chan, C. K.; Zhao, W.; Barlow, S.; Marder, S.; Kahn, A. Decamethylcobaltocene as an Efficient n-Dopant in Organic Electronic Materials and Devices. *Org. Electron.* **2008**, *9*, 575–581.
24. Tian, X. Q.; Xu, J. B.; Wang, X. M. Band Gap Opening of Bilayer Graphene by F4-TCNQ Molecular Doping and Externally Applied Electric Field. *J. Phys. Chem. B* **2010**, *114*, 11377–11381.
25. Sun, J. T.; Lu, Y. H.; Chen, W.; Feng, Y. P.; Wee, A. T. S. Linear Tuning of Charge Carriers in Graphene by Organic Molecules and Charge-Transfer Complexes. *Phys. Rev. B* **2010**, *81*, 155403.
26. Min, H.; Sahu, B.; Banerjee, S. K.; MacDonald, A. H. *Ab initio* Theory of Gate Induced Gaps in Graphene Bilayers. *Phys. Rev. B* **2007**, *75*, 155115.
27. Zhang, W.; Lin, C.-T.; Liu, K.-K.; Tite, T.; Su, C.-Y.; Chang, C.-H.; Lee, Y.-H.; Chu, C.-W.; Wei, K.-H.; Kuo, J.-L.; *et al*. Opening an Electrical Band Gap of Bilayer Graphene with Molecular Doping. *ACS Nano* **2011**, *5*, 7517–7524.
28. Szafranek, B. N.; Schall, D.; Otto, M.; Neumaier, D.; Kurz, H. High On/Off Ratios in Bilayer Graphene Field Effect Transistors Realized by Surface Dopants. *Nano Lett.* **2011**, *11*, 2640–2643.
29. Xia, F.; Farmer, D. B.; Lin, Y.; Avouris, P. Graphene Field-Effect Transistors with High On/Off Current Ratio and Large Transport Band Gap at Room Temperature. *Nano Lett.* **2010**, *10*, 715–718.
30. Duong, D. L.; Lee, S. M.; Chae, S. H.; Ta, Q. H.; Lee, S. Y.; Han, G. H.; Bae, J. J.; Lee, Y. H. Band-Gap Engineering in Chemically Conjugated Bilayer Graphene: *Ab Initio* Calculations. *Phys. Rev. B* **2012**, *85*, 205413.
31. Cuong, N. T.; Otani, M.; Okada, S. Electron-state Engineering of Bilayer Graphene by Ionic Molecules. *Appl. Phys. Lett.* **2012**, *101*, 233106.
32. Gava, P.; Lazzeri, M.; Saitta, A.; Mauri, F. *Ab Initio* Study of Gap Opening and Screening Effects in Gated Bilayer Graphene. *Phys. Rev. B* **2009**, *79*, 165431.
33. Zhao, S. J.; Xue, J. M. Tuning the Band Gap of Bilayer Graphene by Ion Implantation: Insight from Computational Studies. *Phys. Rev. B* **2012**, *86*, 165428.

34. Monkhorst, H. J.; Pack, J. D. Special Points for Brillouin-Zone Integrations. *Phys. Rev. B* **1976**, *13*, 5188–5192.
35. Vosko, S. H.; Wilk, L.; Nusair, M. Accurate Spin-Dependent Electron Liquid Correlation Energies for Local Spin Density Calculations: A Critical Analysis. *Can. J. Phys.* **1980**, *58*, 1200–1211.
36. Girifalco, L.; Hodak, M. van der Waals Binding Energies in Graphitic Structures. *Phys. Rev. B* **2002**, *65*, 125404.
37. Henwood, D.; Carey, J. D. *Ab initio* Investigation of Molecular Hydrogen Physisorption on Graphene and Carbon Nanotubes. *Phys. Rev. B* **2007**, *75*, 245413.
38. Perdew, J.; Burke, K.; Ernzerhof, M. Generalized Gradient Approximation Made Simple. *Phys. Rev. Lett.* **1996**, *77*, 3865–3868.
39. Tkatchenko, A.; Scheffler, M. Accurate Molecular van der Waals Interactions from Ground-State Electron Density and Free-Atom Reference Data. *Phys. Rev. Lett.* **2009**, *102*, 73005.
40. Hirshfeld, F. L. Bonded-atom Fragments for Describing Molecular Charge Densities. *Theor. Chim. Acta* **1977**, *44*, 129–138.